We are IntechOpen, the world's leading publisher of Open Access books Built by scientists, for scientists

6,900
Open access books available

186,000
International authors and editors

200M
Downloads

Our authors are among the

154
Countries delivered to

TOP 1%
most cited scientists

12.2%
Contributors from top 500 universities

CLARIVATE ANALYTICS
BOOK CITATION INDEX
INDEXED

WEB OF SCIENCE™

Selection of our books indexed in the Book Citation Index
in Web of Science™ Core Collection (BKCI)

Interested in publishing with us?
Contact book.department@intechopen.com

Computation of Thermal Conductivity of Gas Diffusion Layers of PEM Fuel Cells

Andreas Pfrang, Damien Veyret and Georgios Tsotridis
European Commission, Joint Research Centre, Institute for Energy
P.O. Box 2, NL-1755 ZG Petten,
The Netherlands

1. Introduction

While fuel cells in general are expected to play a major role in the future energy supply, proton exchange membrane (PEM) fuel cells are considered especially interesting for automotive applications due to their relatively low operating temperature which allows for fast start-up and flexibility in power output. Other promising applications of PEM fuel cells are back-up power units, small portable power supplies, micro combined heat and power installations, but also large scale stationary PEM fuel cell plants.
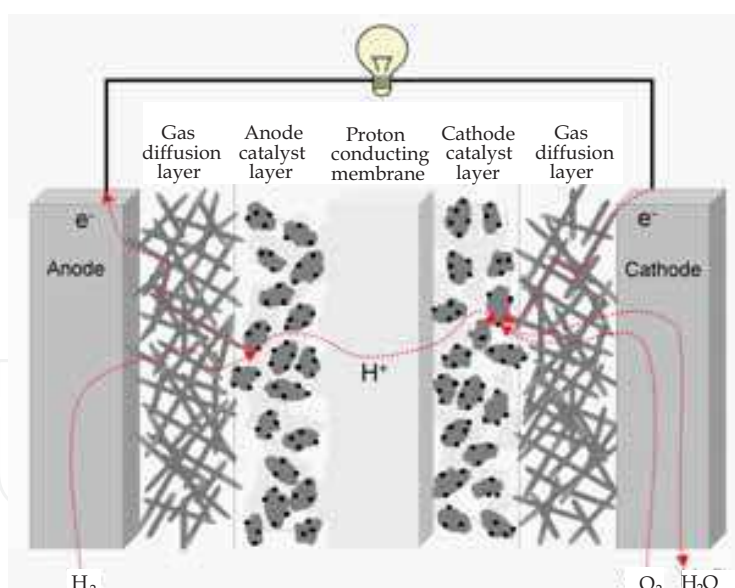

Fig. 1. Sketch of a PEM fuel cell (not to scale). A PEM fuel cell contains two gas diffusion layers, one on the anode and one on the cathode side

Fig. 1 illustrates the principle of a PEM fuel cell. At the anode (left hand side) protons are produced from hydrogen and have to move through the proton-conducting (but not electron-conducting) membrane to the cathode side (right hand side). Electrons will be transported via the electrical load outside the fuel cell to the cathode side where water is produced as 'waste'.

The two gas diffusion layers (GDL) have multiple functions in a PEM fuel cell: provide gas access to the catalyst layers, allow removal of product water on the cathode side while also keeping the membrane and electrode layers humidified when gas conditions are sub-saturated, mechanically stabilize the membrane-electrode assembly while compensating for thickness variations of the membrane, and providing electrical and thermal conductivity.

A GDL has typically a thickness of 200 to 400 μm and consists of carbon fiber papers or carbon fiber felts which are impregnated with polytetrafluoroethylene (PTFE) to achieve a partial hydrophobization of the surfaces (Mathias et al., 2003). Carbon binder can be added for a mechanical joining of neighbouring fibers. Furthermore, a microporous layer (MPL, typical pore sizes around 100 nm) consisting of a mixture of carbon black and PTFE is often applied with a thickness of a few 10 μm on the side facing the catalyst layer for a further optimization of the water management (Paganin et al., 1996; Giorgi et al., 1998; Mathias et al., 2003).

An operating PEM fuel cell is not isothermal, mainly because heat is generated within the membrane electrode assembly and at the same time this assembly can be considered 'insulated' by the gas diffusion layers (Burheim et al., 2011) leading to temperature gradients within the fuel cell. A detailed knowledge of the temperature distribution and therefore of thermal conductivity of the GDLs is essential for a proper understanding and the optimization of not only heat transfer in the PEM fuel cell, but also for water management and optimization of cell performance and durability. A direct measurement of thermal conductivity is possible and has been performed mainly for the through–plane direction (see Table 2). Nevertheless, the direct measurement is for several reasons non-trivial: due to the anisotropy of the GDLs, the thermal conductivity is expected to be anisotropic as well. Furthermore, the through-plane thermal conductivity as well as the contact resistance change with a compression of the GDL (Burheim et al., 2010; Sadeghi et al., 2011a). Recently, the measurement of in-plane thermal conductivities has been reported (Sadeghi et al., 2011b; Teertstra et al., 2011).

Alternatively, the anisotropic thermal conductivity of gas diffusion layers can be calculated based on the 3D microstructure of the GDL and the knowledge of thermal conductivity of the different materials which are present in the GDL. This approach is presented in the following using X-ray computed tomography structure data of gas diffusion layers as well as randomly computer-generated 3D structures based on structural models of gas diffusion layers.

2. Materials and methods

2.1 3D structure of gas diffusion layers

The computation of anisotropic thermal conductivity requires the knowledge of the 3D structure of the gas diffusion layer, i.e. also the 3D distribution of the different materials that are present in the gas diffusion layer. This is especially important as the thermal conductivities of these different materials differ considerably: air 0.026 W m^{-1} K^{-1} (Taine & Petit, 1989) , PTFE 0.25 W m^{-1} K^{-1} (Marotta & Fletcher, 1996) and a typical value for PAN-based carbon fibers with relatively high strength and at the same time relatively high modulus is 120 W m^{-1} K^{-1} (Toray Industries, 2005a).

2.1.1 Characterization of 3D structures by X-ray computed tomography

The first approach presented here is the application of X-ray computed tomography (CT) where a 3D image of an object is determined by digital processing of a large series of two-

dimensional X-ray images taken around a single axis of rotation (see Fig. 2). The 3D image of the object consists of voxels with a certain gray value. Each voxel is then assigned to one material that is present in the object e.g. by considering its gray value. This assignment is denoted as 'segmentation'.
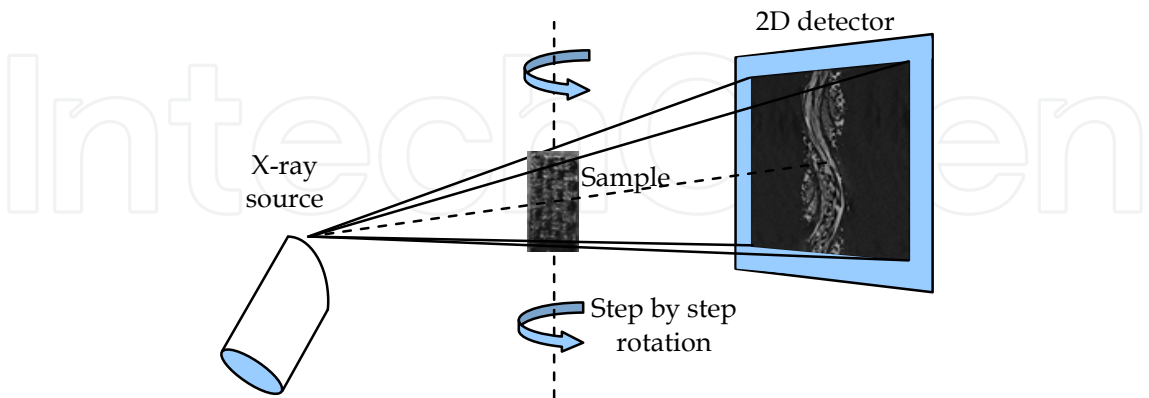

Fig. 2. Principle of X-ray computed tomography (CT). A carbon cloth is shown as sample

X-ray computed tomography (Ostadi et al., 2008; Pfrang et al., 2010) as well as synchrotron based tomography (Becker et al., 2008; Becker et al., 2009) have been used for imaging of gas diffusion layers at resolutions below 1 μm.

Also membranes and membrane electrode assemblies (Garzon et al., 2007; Pfrang et al., 2011) have been imaged by X-ray computed tomography and even functioning fuel cells have been imaged by synchrotron-based methods and soft X-ray radiography e.g. for imaging of liquid water in the GDL (Sinha et al., 2006; Bazylak, 2009; Sasabe et al., 2010; Tsushima & Hirai, 2011).

Gas diffusion layer	PTFE / wt%	Thickness / mm	Porosity
E-Tek, EC-CC1-060T	30	0.33	0.75
E-Tek, EC-TP1-060T	30	0.19	0.72
SGL Carbon, Sigracet 35 BC (with microporous layer)	5	0.325	0.80

Table 1. Properties of gas diffusion layers investigated by X-ray computed tomography (Toray Industries, 2005b; SGL Group, 2009; Pfrang et al., 2010)

Here, CT data from three different commercially available gas diffusion layers will be discussed which were imaged by a nanotom X-ray computed tomography system (GE Sensing and Inspection Technologies, phoenix X-ray, Wunstorf, Germany) at a resolution below 1 μm. Table 1 shows PTFE content, thickness and porosity of the investigated gas diffusion layers. Segmentation into solid material (i.e. carbon and PTFE) and air was carried out based on a gray level threshold. Further details can be found in (Pfrang et al., 2010).

2.1.2 Random generation of 3D structures
The second approach is the random generation of three-dimensional fiber structures using the FiberGeo module of the Geodict software package (Fraunhofer ITWM, 2011). Geometric

parameters such as fiber diameter and length, fiber volume fraction were specified as well as the size of the grid as specified by the number of voxels in x, y and z-direction, n_x, n_y and n_z.

The degree of orientation anisotropy was characterized by the anisotropy parameter β. Using spherical coordinates, β characterizes the directional distribution of fibers. The density of the directional distribution is given by Equation (1), (Schladitz et al., 2006):

$$P(\theta,\phi) = \frac{1}{4\pi} \frac{\beta \sin\theta}{\left(1 + \left(\beta^2 - 1\right)\cos^2\theta\right)} \tag{1}$$

with the inclination $\theta \in [0, \pi)$ and the azimuth $\varphi \in [0, 2\pi)$. The density is thus independent of φ, i.e. the density exhibits rotational symmetry with respect to the z-axis. The case β = 1 describes the isotropic system. For β →∞, the cylinders tend to be more and more parallel to the xy-plane. For β → 0 the cylinders tend to be more and more parallel to the z-axis.

For the randomly generated structures presented here, the selected structure size was 200 x 200 x 271 voxels with a voxel length of 0.7 μm. The fiber volume fraction was 21 % and an anisotropy factor ß of 1000 was chosen. The fibers had a diameter of 10 voxels and were assumed to have infinite length. For further details of the random generation of 3D structures, see also (Veyret & Tsotridis, 2010).

Additionally, model structures consisting of layers of equidistant parallel fibers were generated for the examination of the influence of PTFE distribution on thermal conductivity. For each model structure (see e.g. Fig. 6, before and after the addition of PTFE), the distance between adjacent fiber layers was fixed, but model structures were generated for 6 different layer distances. As the filling factor of the carbon fibers was kept constant at 22 %, the lateral distance between parallel fibers within a layer was adjusted accordingly.

The addition of PTFE to the fiber structures – the randomly generated structures as well as the model structures – was implemented by using the 'add binder'-function in GeoDict, where pores are filled starting from the smallest pores and then continuing to bigger pores until the desired binder volume fraction is reached. The algorithm used here to determine the size of a pore does not distinguish between through pores, closed pores and blind pores and is in this sense purely geometrical. A pore radius is determined by fitting spheres into the pore volume, i.e a point belongs to a pore of radius larger than r, if it is inside any sphere of radius r, which can be fitted into the pore space (Fraunhofer ITWM, 2011).

2.2 Numerical method for the computation of effective thermal conductivity

For the computation of the effective thermal conductivity of fibrous materials, the steady, purely diffusive, three-dimensional heat transfer equation has to be solved. In the case of large three-dimensional geometries (e.g. large data sets from CT imaging, see section 2.1.1 or generated randomly, see section 2.1.2), partial differential equation solvers are not efficient. (Wiegmann & Zemitis, 2006) use a different approach where the energy equation is solved by harmonic averaging. Fast Fourier transform and bi-conjugate gradient stabilized (BiCGStab) methods are then used to solve the Schur-complement formulation. This method – where convection and radiation transport, as well as thermal contact resistance and phase changes are not taken into account – is implemented in the GeoDict software which was also used for the random generation of 3D structures. Further details can be found in (Veyret & Tsotridis, 2010).

Whereas in the randomly generated 3D structures the distribution of PTFE and carbon is well known, these two materials could not be distinguished in the CT data. As a rough approximation, all solid voxels in the CT datasets were assumed to have a thermal conductivity that was calculated as the weighted average of the thermal conductivities of the carbon fibers and the thermal conductivity of PTFE, even though these two materials do not intermix. The remaining, non-solid voxels were assumed to be filled with air.

3. Results and discussion

3.1 Estimation of thermal conductivity of heterogeneous materials

Several analytical models for the estimation of thermal conductivity of heterogeneous materials exist (Progelhof et al., 1976; Carson et al., 2005; Wang et al., 2006) and can be applied to gas diffusion layers. In the following, the most fundamental models – parallel model, series model, Maxwell Eucken model, effective medium theory model and co-continuous model – are presented. Furthermore it is possible to use combinations of two or more of these fundamental models for the estimation of thermal conductivity (Krischer, 1963; Wang et al., 2006).

If conduction is the only or the dominating heat transfer mechanism, it may be assumed that thermal conductivity of a porous material will lie between the parallel and series model values. Equation (2) describes the result using the parallel model which considers the thermal resistances to be in parallel, i.e. heat can flow through both materials in parallel. The parallel model gives the upper bound of effective thermal conductivity of the heterogeneous material.

$$k_{h,p} = fk_s + (1-f)k_{air} \tag{2}$$

k_h is the thermal conductivity of the heterogeneous material; the second subscript denotes the model used for its estimation (e.g. p for parallel). f is the filling factor i.e. the volume fraction of the solid phase, k_s is the thermal conductivity of the solid phase and k_{air} the thermal conductivity of air. The volume fraction of air is 1-f.

In the series model (see equation (3)), the thermal resistances are considered to be in series with respect to the heat flux and $k_{h,s}$ gives the lower bound of effective thermal conductivity.

$$k_{h,s} = \frac{1}{f/k_s + (1-f)/k_{air}} \tag{3}$$

The effective medium theory (EMT) model (see equation (4)) assumes a random, mutual dispersion of two components (Carson et al., 2005).

$$k_{h,EMT} = \frac{1}{4}\left((3f-1)k_s + (2-3f)k_{air} + \sqrt{\left[(3f-1)k_s + (2-3f)k_{air}\right]^2 + 8k_{air}k_s} \right) \tag{4}$$

Equation (5) shows the result of the co-continuous model (Wang et al., 2008) where both phases are assumed to be continuous.

$$k_{h,C-C} = \frac{k_{h,s}}{2}\left(\sqrt{1 + 8k_{h,p}/k_{h,s}} - 1 \right) \tag{5}$$

Even though this model is independent of parallel and series model, the result $k_{h,\,C\text{-}C}$ can be expressed as function of $k_{h.\,p}$ and $k_{h,\,s}$, which are the thermal conductivities calculated for the parallel and series model (see equations (2) and (3)).

Whereas all four models mentioned so far are symmetric with respect to exchange of the two phases, the Maxwell-Euken model (Eucken, 1940) is not, as one phase is assumed to be dispersed in a second, continuous phase. The heterogeneous conductivity calculated following the Maxwell-Euken model $k_{h,\,M\text{-}E}$ is given in (6) where the index 'cont' refers to the continuous phase and the index 'dis' to the dispersed phase.

$$k_{h,\,M\text{-}E} = \frac{k_{cont}f_{cont} + k_{dis}f_{dis}\dfrac{3k_{cont}}{2k_{cont} + k_{dis}}}{f_{cont} + f_{dis}\dfrac{3k_{cont}}{2k_{cont} + k_{dis}}} \tag{6}$$

Obviously, each of the models assumes a certain geometry which does not reflect exactly the microstructure of a GDL. Gas diffusion layers typically exhibit anisotropy of the microstructure as carbon fibers are preferentially oriented in–plane. Furthermore, carbon fibers are expected to exhibit an anisotropic thermal conductivity as e.g. pyrolytic graphite (Wen & Huang, 2008) – the degree of anisotropy depending on the type of fiber – due to their anisotropic, partly graphite-like structure. Both, the anisotropy in microstructure and the anisotropy of thermal conductivity in carbon fibers is not into account in any of the presented models.
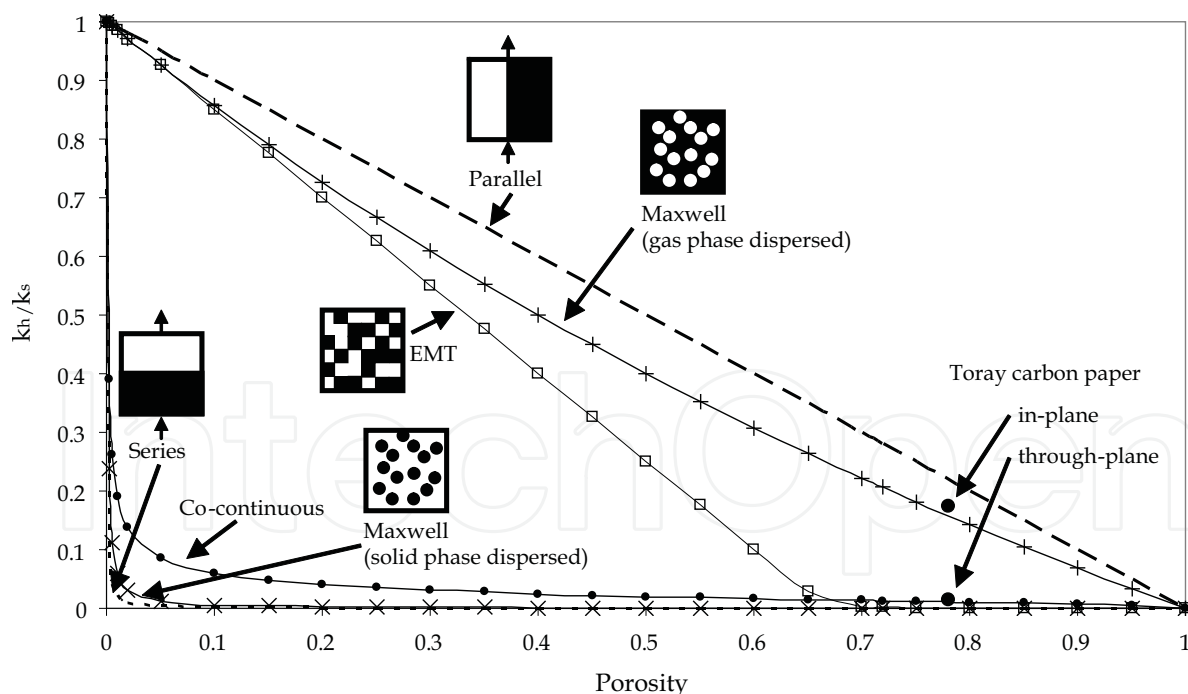

Fig. 3. Estimated thermal conductivity of the heterogeneous material k_h normalized with respect to the thermal conductivity of the solid phase k_s dependent on porosity. Different models were used for the estimation using a ratio of k_s/k_{air} of 120 Wm^{-1}K^{-1} / 0.026 Wm^{-1}K^{-1}. For some models, the assumed structure is shown as insert; the small arrows indicate the direction of heat flux where appropriate. Additionally, the thermal conductivity of Toray carbon paper as given by the manufacturer (Toray Industries, 2005b) is shown

Nevertheless, the models can be applied to gas diffusion layers and Fig. 3 shows normalized thermal conductivity estimated using the models mentioned above assuming a ratio of thermal conductivities k_s/k_{air} of 120 $Wm^{-1}K^{-1}$ / 0.026 $Wm^{-1}K^{-1}$ which is an estimate for gas diffusion layers consisting of carbon fibers in air. As an example of a GDL, the in-plane and through-plane thermal conductivities of Toray carbon paper without the addition of PTFE as given by the manufacturer (Toray Industries, 2005b) are included assuming a k_s of 120 $Wm^{-1}K^{-1}$.

Overall, the presented models allow estimating the order of magnitude of the thermal conductivity of gas diffusion layers, but – also due to the anisotropic microstructure of a typical GDL – a more precise a-priori estimation seems impossible.

3.2 Computation of thermal conductivity of gas diffusion layers

As more accurate thermal conductivity data is required, one further approach is the computation based on 3D structure data (Becker et al., 2008; Pfrang et al., 2010; Veyret & Tsotridis, 2010; Zamel et al., 2010). Fig. 4 illustrates the two approaches applied here: the characterization of GDL 3D structure by X-ray computed tomography (section 2.1.1), left and the random generation of 3D models of the GDL structure (section 2.1.2), right. Both approaches have certain advantages and drawbacks: While the randomly generated structures allow an accurate definition of the distribution of each material, in CT it was not possible to discriminate carbon from PTFE due to similar X-ray adsorption. CT, on the other hand, provides the realistic 3D structure; whereas there are deviations from the real structure after random structure generation (e.g. straight fibers are assumed). In both approaches there are limitations with respect to spatial resolution; resolution of X-ray CT is limited while essentially computer hardware and computing time limit the number of voxels of randomly generated structures.

Even though PTFE cannot be discriminated from carbon fibers by the contrast in the CT datasets, the carbon fibers are clearly visible in the 3D structure (see top left of Fig. 4) and the micro porous layer (MPL) is clearly visible in the cross-section (see bottom left of Fig. 4).

For one of the samples investigated by CT – EC-TP1-060T – a corresponding randomly generated structural model was generated. This sample was selected as it contains relatively straight fibers (as compared to the carbon cloth) and does not contain a micro porous layer. The parameters for the structure generation were chosen according to the manufacturer's datasheet (Toray Industries, 2005b): 22 % filling factor of carbon; these 22 % were distributed into 21 % carbon fiber and 1 % carbon binder. After fiber generation and addition of the carbon binder, 30 wt. % of PTFE were added.

The results are given in Table 2 with gray background together with a selection of thermal conductivity data published in the literature. For in-plane thermal conductivity, two values are given if the thermal conductivity was determined independently for two orthogonal in-plane directions, and one value is given when the average in-plane conductivity was determined.

In an earlier study (Ihonen et al., 2004), thermal conductivity for several types of GDLs was estimated to 0.2-0.4 W/m K, which was considered unrealistically low in the study. Nevertheless, this estimated range is in agreement with more recent measurements. Finally, a study on the computation of thermal conductivity based on model structures with different geometries was published by (Zamel et al., 2010) where the calculated values are given relative to the thermal conductivity of the solid phase and therefore the values are not given in Table 2. It is reasonable to give this ratio, because the thermal conductivity of carbon fibers is often not known as it depends on the type of carbon fiber and can vary by

orders of magnitude (Blanco et al., 2002) depending e.g. on the heat treatment of the fibers. This may explain the apparent discrepancy between the results for structural models of carbon paper by (Becker et al., 2008) and (Veyret & Tsotridis, 2010) where thermal conductivity values of 17 W/ m K and 130 W/ m K were used, respectively.

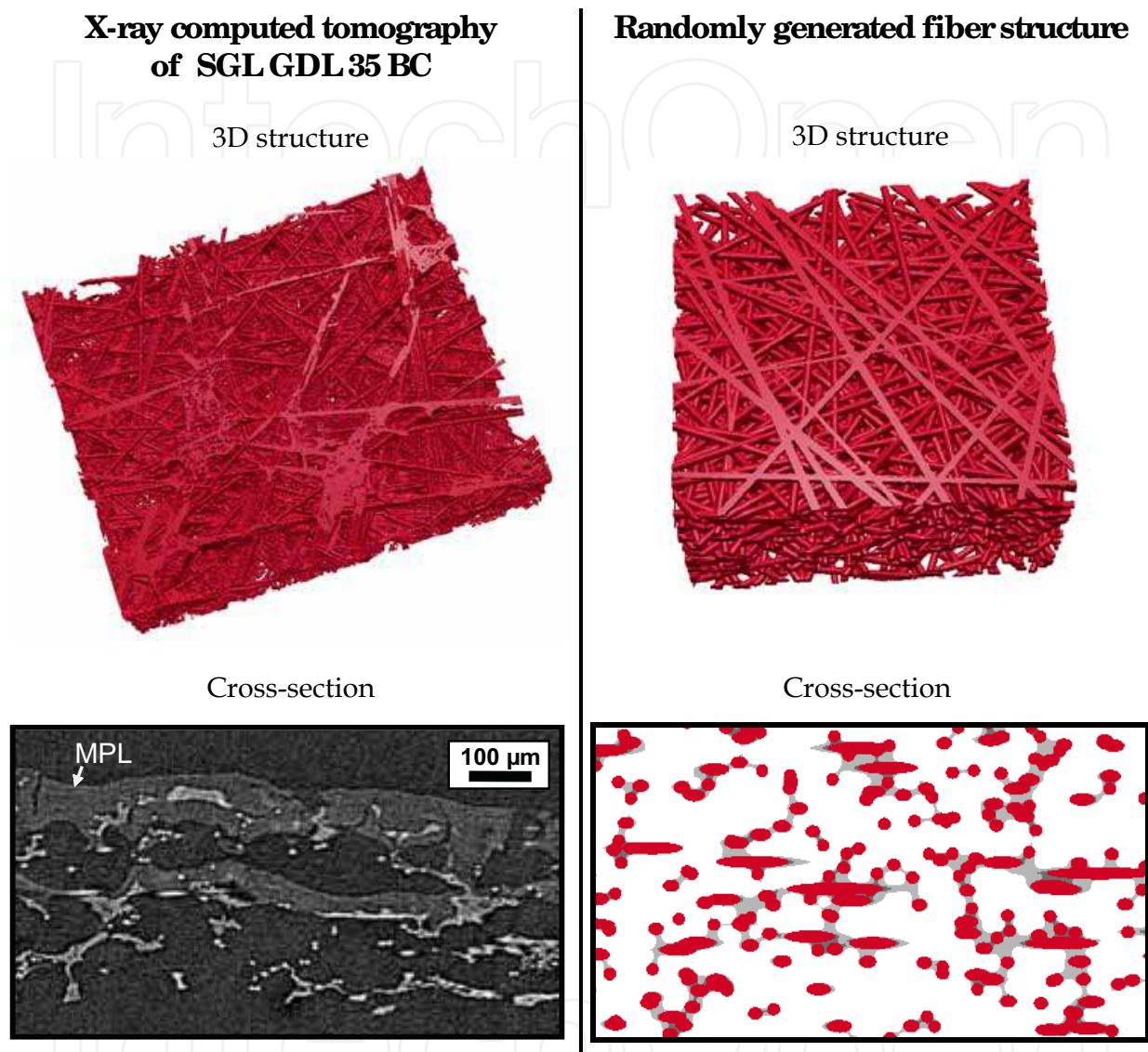| **X-ray computed tomography of SGL GDL 35 BC**	**Randomly generated fiber structure**
3D structure	3D structure

Fig. 4. 3D structure and cross-section of a GDL as determined by X-ray computed tomography (left) and randomly generated (right). The micro porous layer (MPL) is clearly visible in the CT cross section. In the 3D structure of the randomly generated structure only the carbon fibers are shown (not carbon binder and PTFE), while in the cross section, the fibers (red) can be clearly discriminated from carbon binder (dark gray) and PTFE (light gray)

The focus of earlier work was on through-plane thermal conductivity of the GDL, as the heat flows predominantly through-plane in a PEM fuel cell. Nevertheless, for a detailed understanding of the heat flux, also in-plane thermal conductivity is relevant, e.g. because thermal contact between bipolar plate and GDL is not homogeneous due to the gas flow channels in the bipolar plate. Only recently measurements of in-plane thermal conductivity were published (Sadeghi et al., 2011b; Teertstra et al., 2011).

When considering all data from Table 2, the range of thermal conductivity values for the through-plane direction is 0.13-2.8 W / m K, as compared to a range of 1.75-21 W / m K for the in-plane direction. As carbon fibers have a higher thermal conductivity than PTFE or air, this can be explained by the preferred orientation of the carbon fibers in-plane, i.e. heat can be transported mainly along the fibers in-plane, whereas for through-plane heat transfer from fiber to fiber is required to a larger extent.

In a PEM fuel cell, the GDL is subject to compression and consequently in most experimental setups used for the determination of thermal conductivity the GDL is investigated under compression. As a general trend, an increase of thermal conductivity and a reduction of thermal resistance were found with increasing compression. More recently, also the effect of load cycling – i.e. cycles of increasing compression up to a maximum value and releasing compression to 0 – was investigated and steady-state (in the investigated case reached after 5 cycles) properties were determined (Sadeghi et al., 2010).

Further, it was found that residual water in the GDL leads to a significant increase of through-plane thermal conductivity (Burheim et al., 2010; Burheim et al., 2011). The influence of PTFE distribution on thermal conductivity is discussed in section 3.3.

In the following paragraphs, our data on thermal conductivity will be compared with literature data. For the computation for E-Tek EC-CC1-060T, only one measurement on a similar sample – but without PTFE – is available and gives a clearly lower thermal conductivity. One explanation could be that the addition of PTFE leads to an increase of thermal conductivity, but this is not in accordance with the trend of a decrease of thermal conductivity observed for other samples. Because PTFE cannot be discriminated from carbon fibers in the CT dataset, it seems reasonable to assume that the thermal contact between fibers is overestimated in our computation (as an arithmetic average of thermal conductivity between carbon and PTFE was used in the computation for all solid voxels) which results in an overestimation of thermal conductivity.

For Sigracet 35 BC, the MPL was not considered in the computation of thermal conductivity, i.e. it was replaced by air. This obviously leads to an overall underestimation of thermal conductivity as observed.

One way forward would be the clear identification of MPL material (maybe applying advanced segmentation techniques or using improved CT imaging techniques) and its inclusion into the computation.

When comparing our results computed from the CT data of EC-TP1-060T and the randomly generated model (based on EC-TP1-060T), through-plane thermal conductivities agree well - 1.7 vs. 1.65 W / m K – whereas in-plane thermal conductivities are significantly larger for the randomly generated model. The in-plane heat flux is expected to flow mainly along the fibers. Therefore the different thermal conductivities assumed for solid voxels – 120 W / m K for the carbon fibers in the randomly generated model vs. 93 W / m K as weighted average between carbon and PTFE for the CT dataset – could explain this difference. Nevertheless, the computed thermal conductivities lie well within the range of values available in the literature for Toray carbon paper based materials for through-plane as well as in-plane direction.

3.3 Influence of PTFE distribution

Experimental results have shown that an increase of PTFE loading leads to a reduction of through-plane thermal conductivity (Khandelwal & Mench, 2006; Burheim et al., 2011) in several, but not all types of gas diffusion layers (see Table 2).

Table 2. (continues) Published values of thermal conductivity of gas diffusion layers

Gas diffusion layer	PTFE / %	Thermal conductivity / W m⁻¹ K⁻¹ through-plane	in-plane	Remarks	Type of data	Technic
E-Tek EC-CC1-060	0	0.28-0.32		4.6-13.9 bar compression dry GDL	ex situ	unidirectional heat flux and differen
E-Tek EC-CC1-060T	30	1.4	5.6, 6.2	based on x-ray CT data	computation	EJ-Heat solver (Wiegma
E-Tek ELAT carbon cloth LT1200-W, thickness 275 um	0	0.22			ex situ	unidirectional heat flux and differen
E-Tek ELAT carbon cloth, thickness 180 μm	0	0.2		combined value for catalyst surface + GDL	in situ	calculated from temperature p
E-Tek ELAT carbon cloth, thickness 410 μm	not av.	0.13-0.19			in situ	estimated from temperature c cell
Freudenberg FCCT H2315	0	0.14-0.15		4.6-13.9 bar compression dry GDL	ex situ	unidirectional heat flux and differen
Freudenberg FCCT H2315 T10A	10	0.15-0.16				
SGL Sigracet 10 AA	0	0.30-0.42		4.6-13.9 bar compression dry GDL	ex situ	unidirectional heat flux and differen
	0	0.7-0.87		4.6-13.9 bar compression residual water		
SGL Sigracet 10 BA	5	0.26-0.33		4.6-13.9 bar compression dry GDL	ex situ	unidirectional heat flux and differen
	5	1.18		conductivity almost independent of compression up to 5.5 MPa	ex situ	unidirectional heat flux and differen
SGL Sigracet 24 AA	0	0.48				
SGL Sigracet 24 BA	5	0.31			ex situ	unidirectional heat flux and differen
SGL Sigracet 24 DA	20	0.22				
SGL Sigracet 25BC and 35BC	5	0.6-0.9		0.04-1.3 MPa compression	ex situ	guarded hot plate, two simil thicknesses
SGL Sigracet 35 BC	5	0.16	1.9, 2.0	based on x-ray CT data (without MPL)	computation	EJ-Heat solver (Wiegma
SGL Carbon, thickness 420 μm	yes	0.26-0.34		estimate based on experiment	ex situ	unidirectional heat flux and differen
SolviCore carbon paper	30	0.25-0.52		0.7 - 13.8 bar compression	ex situ	ASTM Standard D-5470-(unidirectional
	30		3.2-3.87	in vacuum	ex situ	thermal resistance measurer thermal conductance
	not av.	0.27-0.40		4.6-13.9 bar compression dry GDL	ex situ	unidirectional heat flux and differen
		0.45-0.57		4.6-13.9 bar compression residual water		
SpectraCarb carbon paper	0	0.26-0.7		0.7 - 13.8 bar compression	ex situ	ASTM Standard D-5470-(unidirectiona
	12, 19, 29	0.28-0.6				
	0		12.8, 13.8	in vacuum	ex situ	thermal resistance measurer thermal conductance
	6, 11, 19		9.78-14.2			

Table 2. (continued) (results by the authors marked by gray background)

Gas diffusion layer	PTFE /%	Thermal conductivity / W m^{-1} K^{-1}		Remarks	Type of data	Techni
		through-plane	in-plane			
Toray carbon paper TGP-H-060	0	2.8		compression 1.9 MPa	in situ	estimated from temperature c cell
	0	1.8-1.2		temperature 26 - 73 °C	ex situ	unidirectional heat flux and differer
	5	0.41-0.66		4.6-13.9 bar compression dry GDL	ex situ	unidirectional heat flux and differer
		1.6		4.6-13.9 bar compression residual water		
E-Tek EC-TP1-060T based on Toray TGP-H-060	30	1.7	8.9, 8.0	based on x-ray CT data	computation	EJ-Heat solver (Wiegma
Carbon paper EC-TP1-060T (structural model)	30	1.65	13.8	based on structural model	computation	EJ-Heat solver (Wiegma
Toray carbon paper, Quintech, thickness 190 μm	0	0.36-1.36		estimate based on experiment	ex situ	unidirectional heat flux and differer
Toray carbon paper, Quintech, thickness 230 μm	yes	0.20-0.30				
Toray carbon paper TGP-H-060 / -090 and -120	0	1.7	21		datasheet	not avail
Toray carbon paper TGP-H-060 and -120	0	1.6-1.9		0.04-1.3 MPa compression	ex situ	guarded hot plate, two simila thicknesses
	5	1.4-2.1		0.2-1.5 MPa compression	ex situ	unidirectional heat flux and differer
Toray carbon paper TGP-H-090	5	1.4-1.5		4.6-13.9 bar compression residual water	ex situ	unidirectional heat flux and differer
		0.5-0.73		4.6-13.9 bar compression dry GDL		
	10	0.48-0.69				
	60	0.28-0.32				
Toray carbon paper, Quintech, thickness 280 μm	0	0.33-0.59		estimate based on experiment	ex situ	unidirectional heat flux and differer
Toray carbon paper TGP-H-120	5	0.62-0.89		4.6-13.9 bar compression dry GDL	ex situ	unidirectional heat flux and differer
		1.4		4.6-13.9 bar compression residual water		
	5	1.55-2.1		at quasi steady state, load cycling 0.25-1.5 MPa, in vacuum	ex situ	unidirectional heat flux and differer
	5-30		17.3-17.8	in vacuum	ex situ	thermal resistance measurem of different
	30		15.1	in vacuum	ex situ	thermal resistance measure thermal conductance
Carbon paper (structural model)	≤ 20	0.296	1.75, 2.05	based on synchrotron 3D structure data	computation	EJ-Heat solver (Wiegma
		0.388	2.55	compressed by 20%, based on synchrotron 3D structure data		
Carbon paper (structural model)	0	1.86	9.79, 9.82	based on structural model	computation	EJ-Heat solver (Wiegma
	0-25	1.86-1.2				

Assuming that the structure of the GDL remains unchanged, one would expect that the addition of material that has a higher thermal conductivity than air – like PTFE – should increase the overall thermal conductivity.
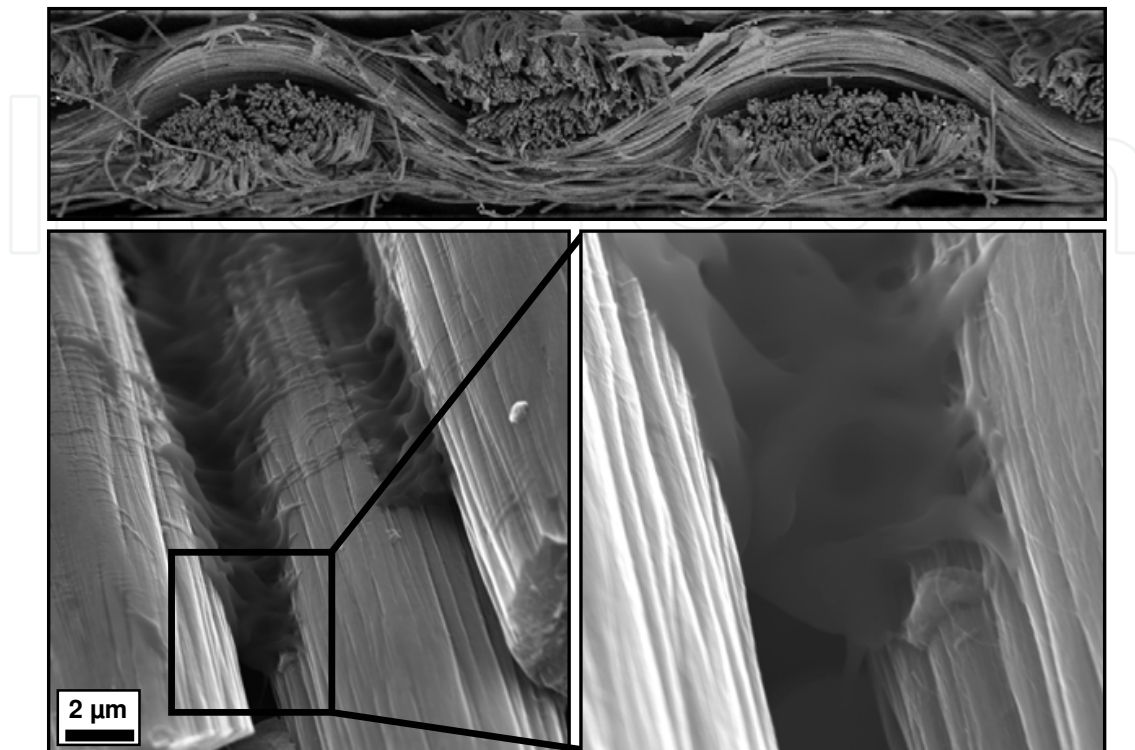

Fig. 5. Scanning electron micrographs of the cross section of carbon cloth EC-CC1-060T: the top image gives an overview of the whole thickness of the cross section, the bottom two images show carbon fibers with PTFE in between

However, since the thermal conductivity of PTFE is orders of magnitude smaller than that of carbon, PTFE potentially can insulate carbon fibers from each other, i.e. the contact region between carbon fibers can have a big impact on the thermal conductivity of the GDL. This is especially relevant for carbon papers where the carbon fibers are oriented preferably in-plane, which means that through-plane heat transfer requires heat transfer from fiber to fiber. Fig. 5 shows scanning electron micrographs of the cross section of carbon cloth EC-CC1-060T. In the selected region, PTFE separates two neighbouring carbon fibers. For a further illustration of this possible insulation effect, thermal conductivity of model structures of layers of parallel fibers with a filling factor of 22 % were randomly generated using GeoDict (see Fig. 6). Model structures with different distances between the fiber layers were investigated and thermal conductivity of each of these structures was evaluated without PTFE and after the addition of 30 wt. % of PTFE. These model structures are surely not a realistic description of any GDL, but they will be used to examine different possible geometries of the contact region between fibers. As these fibers are oriented exactly in-plane, the model structures represent an extreme case with respect to through-plane conductivity in the sense that heat transfer along the fibers cannot contribute significantly.

The computed thermal conductivities of these model structures are summarized in Fig. 7. For the case of touching fibers (distance 0 μm), there is only a small increase in thermal conductivity due to the addition of PTFE around the contact region between fibers.
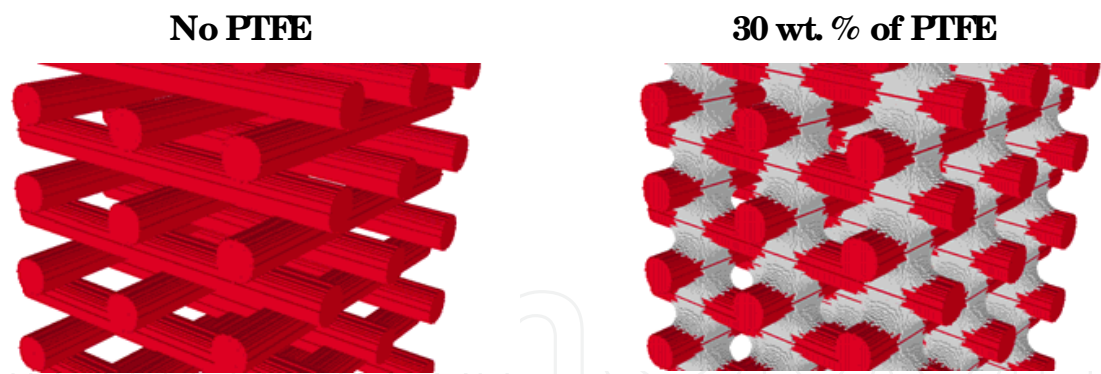
No PTFE   **30 wt. % of PTFE**

Fig. 6. Detail of model structures of layers of equidistant parallel fibers. The filling factor of the carbon fibers is 22 %. Without PTFE (left) and with 30 wt. % of PTFE shown in gray (right)
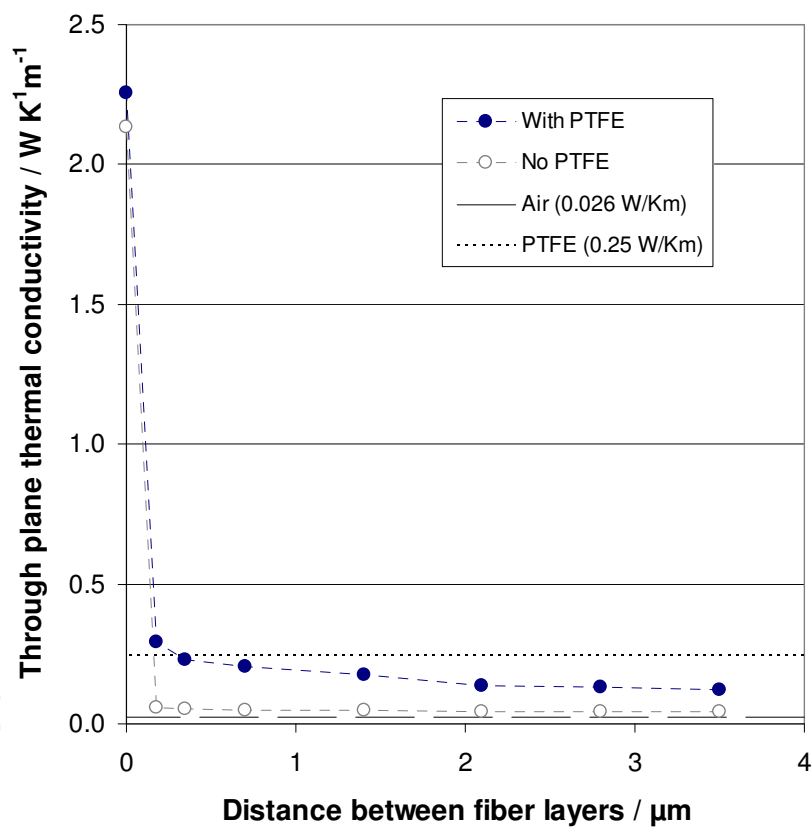
Fig. 7. Computed through-plane thermal conductivity dependent on the distance between fiber layers (based on model structures as illustrated in Fig. 6). For comparison, the thermal conductivities of pure air and pure PTFE are included into the graph

In both cases, with and without PTFE, the conductivity drops sharply from distance 0, i.e. contact between the fibers layers, to a distance of 0.175 μm, the smallest considered distance. For the model structures without PTFE, the conductivity drops to values close to the thermal conductivity of air. These cases are of course not realistic for a GDL as fibers will always be in contact due to the compression of the GDL, but it is illustrated that heat transfer between non-touching fibers is strongly inhibited.

For the model structures with PTFE, the conductivity drops to values below the thermal conductivity of PTFE, which is in the same order of magnitude as thermal conductivities measured for realistic gas diffusion layers (compare Table 2).

It has to be mentioned that in the model structures the contact area between touching fibers (distance 0 μm) was defined by the voxel size of the model structures. It is clear that this contact area will have a huge impact on heat flux through the contact. In this context, the presence of carbon binder – which is used for the mechanical stabilization of the GDL – can play an important role.

Overall, it is obvious from the results presented in Fig. 7 that the contact region between fibers is important for the thermal conductivity of a GDL. When looking back to the models estimating thermal conductivity of heterogeneous materials (section 2.1) and considering the contact area between fibers consisting of PTFE and carbon, both extreme cases – parallel heat flux through carbon and PTFE and heat flux in series through the two components – seem to be potentially realistic for the description of a specific single contact between two fibers in a gas diffusion layer. The macroscopic thermal conductivity of a GDL will depend strongly on the statistical distribution of the different contact geometries.

Considering the drop of thermal conductivity with the increase of PTFE loading observed experimentally, it might be speculated that PTFE can be introduced between fibers thereby reducing the direct contact area between fibers which would explain the observed drop in thermal conductivity. Of course compression as well as mechanical cycling potentially can lead to a modification of contacts between fibers, i.e. the statistical distribution of contact geometries and thereby thermal conductivity could change. Reversible as well as irreversible modifications of contact geometries – and consequently thermal conductivity could occur under mechanical loading.

Also the observation that the presence of residual liquid water leads to an increase of through-plane thermal conductivity (Burheim et al., 2011) can possibly be explained; the water – with a thermal conductivity of 0.6 W/ m K (Taine & Petit, 1989) – could either improve heat flux at already existing contacts between fibers or even provide new heat flux paths that were 'insulated' by air before the addition of water.

4. Conclusion

Three commercially available gas diffusion layers of PEM fuel cells were investigated by 3D X-ray computed tomography (CT). The 3D structure of carbon fiber based gas diffusion layers was clearly resolved, but carbon fibers and PTFE could not be discriminated. Further, 3D fiber structures were randomly generated using GeoDict and model structures of layers of equidistant parallel fibers were generated. Binder material – this could be PTFE only or carbon and PTFE – was added to these fiber structures.

The application of analytical models for the estimation of thermal conductivity of heterogeneous materials was discussed. Based on the measured and generated 3D structures, the macroscopic, anisotropic effective thermal conductivities of the gas diffusion layers were computed. The average in-plane thermal conductivity for all structures is by about a factor 4 to 12 larger than the average through-plane thermal conductivity. These results were compared with the available literature data on thermal conductivity of gas diffusion layers and a good agreement was found.

Finally, it was shown that – due to the big difference between the thermal conductivities of PTFE and carbon – the impact of the contact area between carbon fibers and the spatial

distribution of PTFE in the contact region between carbon fibers on the macroscopic thermal conductivity is considerable. Therefore an improved characterisation of the contact region between carbon fibers could be a worthwhile objective for future similar studies. This includes also the discrimination of PTFE and carbon in CT datasets.

Overall, it was shown that the computation of thermal conductivity of gas diffusion layers based on 3D structure can lead to an improved understanding of the thermal properties of a GDL. Both approaches presented here have advantages: CT measurements guarantee a realistic 3D structure, while the random generation of 3D structures allows the precise definition of the distribution of all components which can be especially relevant for virtual GDL design.

5. Acknowledgment

6. References

Bazylak, A. (2009). Liquid water visualization in PEM fuel cells: A review. *International Journal of Hydrogen Energy* Vol. 34, No. 9, pp. 3845-3857, ISSN 03603199

Becker, J., Flückiger, R., Reum, M., Büchi, F. N., Marone, F. & Stampanoni, M. (2009). Determination of material properties of gas diffusion layers: Experiments and simulations using phase contrast tomographic microscopy. *Journal of the Electrochemical Society* Vol. 156, No. 10, pp. B1175-B1181, ISSN 00134651

Becker, J., Schulz, V. & Wiegmann, A. (2008). Numerical determination of two-phase material parameters of a gas diffusion layer using tomography images. *Journal of Fuel Cell Science and Technology* Vol. 5, No. 2, pp. art. no. 021006, ISSN 1550624X

Blanco, C., Appleyard, S. P. & Rand, B. (2002). Study of carbon fibres and carbon-carbon composites by scanning thermal microscopy. *Journal of Microscopy* Vol. 205, No. 1, pp. 21-32, ISSN 00222720

Burford, D. J. & Mench, M. M. (2004). *Heat transport and temperature distribution in PEFCS.* American Society of Mechanical Engineers, Heat Transfer Division, Anaheim, CA.

Burheim, O. S., Pharoah, J. G., Lampert, H., Vie, P. J. S. & Kjelstrup, S. (2011). Through-plane thermal conductivity of PEMFC porous transport layers. *Journal of Fuel Cell Science and Technology* Vol. 8, No. 2, ISSN 1550624X

Burheim, O. S., Vie, P. J. S., Pharoah, J. G. & Kjelstrup, S. (2010). Ex situ measurements of through-plane thermal conductivities in a polymer electrolyte fuel cell. *Journal of Power Sources* Vol. 195, No. 1, pp. 249-256, ISSN 03787753

Carson, J. K., Lovatt, S. J., Tanner, D. J. & Cleland, A. C. (2005). Thermal conductivity bounds for isotropic, porous materials. *International Journal of Heat and Mass Transfer* Vol. 48, No. 11, pp. 2150-2158, ISSN 00179310

Eucken, A. (1940). Allgemeine Gesetzmässigkeiten für das Wärmeleitvermögen verschiedener Stoffarten und Aggregatzustände. *Forschung auf dem Gebiete des Ingenieurwesens* Vol. 11, No. 1, pp. 6-20, ISSN 00157899

Fraunhofer ITWM (2011). GeoDict, In: *Homepage of the GeoDict software*, 16 February 2011, Available from: www.geodict.com

Garzon, F. H., Lau, S. H., Davey, J. R. & Borup, R. L. (2007). *Micro and nano X-ray tomography of PEM fuel cell membranes after transient operation*. ECS Transactions, Washington, DC.

Giorgi, L., Antolini, E., Pozio, A. & Passalacqua, E. (1998). Influence of the PTFE content in the diffusion layer of low-Pt loading electrodes for polymer electrolyte fuel cells. *Electrochimica Acta* Vol. 43, No. 24, pp. 3675-3680, ISSN 00134686

Ihonen, J., Mikkola, M. & Lindbergh, G. (2004). Flooding of gas diffusion backing in PEFCs: Physical and electrochemical characterization. *Journal of the Electrochemical Society* Vol. 151, No. 8, pp. A1152-A1161, ISSN 00134651

Karimi, G., Li, X. & Teertstra, P. (2010). Measurement of through-plane effective thermal conductivity and contact resistance in PEM fuel cell diffusion media. *Electrochimica Acta* Vol. 55, No. 5, pp. 1619-1625, ISSN 00134686

Kawase, M., Inagaki, T., Kawashima, S. & Miura, K. (2009). *Effective thermal conductivity of gas diffusion layer in through-plane direction*. ECS Transactions, Vienna.

Khandelwal, M. & Mench, M. M. (2006). Direct measurement of through-plane thermal conductivity and contact resistance in fuel cell materials. *Journal of Power Sources* Vol. 161, No. 2, pp. 1106-1115, ISSN 03787753

Krischer, O. (1963). *Die wissenschaftlichen Grundlagen der Trocknungstechnik*, Springer, ISBN 3-540-03018-2, Berlin

Marotta, E. E. & Fletcher, L. S. (1996). Thermal contact conductance of selected polymeric materials. *Journal of Thermophysics and Heat Transfer* Vol. 10, No. 2, pp. 334-342, ISSN 08878722

Mathias, M. F., Roth, J., Fleming, J. & Lehnert, W. (2003). Diffusion media materials and characterisation, In: *Handbook of Fuel Cells - Fundamentals, Technology and Applications, Volume 3*, Vielstich, W., Gasteiger, H. A. & Lamm, A., pp. 517-537, John Wiley, ISBN 0-471-49926-9, Chichester

Nitta, I., Himanen, O. & Mikkola, M. (2008). Thermal conductivity and contact resistance of compressed gas diffusion layer of PEM fuel cell. *Fuel Cells* Vol. 8, No. 2, pp. 111-119, ISSN 16156846

Ostadi, H., Jiang, K. & Prewett, P. D. (2008). Micro/nano X-ray tomography reconstruction fine-tuning using scanning electron microscope images. *Micro and Nano Letters* Vol. 3, No. 4, pp. 106-109, ISSN 17500443

Paganin, V. A., Ticianelli, E. A. & Gonzalez, E. R. (1996). Development and electrochemical studies of gas diffusion electrodes for polymer electrolyte fuel cells. *Journal of Applied Electrochemistry* Vol. 26, No. 3, pp. 297-304, ISSN 0021891X

Pfrang, A., Veyret, D., Janssen, G. J. M. & Tsotridis, G. (2011). Imaging of membrane electrode assemblies of proton exchange membrane fuel cells by X-ray computed tomography. *Journal of Power Sources* Vol. 196, No. 12, pp. 5272-5276, ISSN 03787753

Pfrang, A., Veyret, D., Sieker, F. & Tsotridis, G. (2010). X-ray computed tomography of gas diffusion layers of PEM fuel cells: Calculation of thermal conductivity. *International Journal of Hydrogen Energy* Vol. 35, No. 8, pp. 3751-3757, ISSN 03603199

Progelhof, R. C., Throne, J. L. & Ruetsch, R. R. (1976). Methods for predicting the thermal conductivity of composite systems: a review. *Polymer Engineering and Science* Vol. 16, No. 9, pp. 615-625, ISSN 00323888

Radhakrishnan, A. (2009). *Thermal conductivity measurement of gas diffusion layer used in PEMFC*. Rochester Institute of Technology, Rochester.

Ramousse, J., Didierjean, S., Lottin, O. & Maillet, D. (2008). Estimation of the effective thermal conductivity of carbon felts used as PEMFC gas diffusion layers. *International Journal of Thermal Sciences* Vol. 47, No. 1, pp. 1-6, ISSN 12900729

Sadeghi, E., Djilali, N. & Bahrami, M. (2010). Effective thermal conductivity and thermal contact resistance of gas diffusion layers in proton exchange membrane fuel cells. Part 2: Hysteresis effect under cyclic compressive load. *Journal of Power Sources* Vol. 195, No. 24, pp. 8104-8109, ISSN 03787753

Sadeghi, E., Djilali, N. & Bahrami, M. (2011a). Effective thermal conductivity and thermal contact resistance of gas diffusion layers in proton exchange membrane fuel cells. Part 1: Effect of compressive load. *Journal of Power Sources* Vol. 196, No. 1, pp. 246-254, ISSN 03787753

Sadeghi, E., Djilali, N. & Bahrami, M. (2011b). A novel approach to determine the in-plane thermal conductivity of gas diffusion layers in proton exchange membrane fuel cells. *Journal of Power Sources* Vol. 196, No. 7, pp. 3565-3571, ISSN 03787753

Sasabe, T., Tsushima, S. & Hirai, S. (2010). In-situ visualization of liquid water in an operating PEMFC by soft X-ray radiography. *International Journal of Hydrogen Energy* Vol. 35, No. 20, pp. 11119-11128, ISSN 03603199

Schladitz, K., Peters, S., Reinel-Bitzer, D., Wiegmann, A. & Ohser, J. (2006). Design of acoustic trim based on geometric modeling and flow simulation for non-woven. *Computational Materials Science* Vol. 38, No. 1, pp. 56-66, ISSN 09270256

SGL Group (2009). Sigracet GDL 34 & 35 series gas diffusion layer, In: *Sigracet Fuel Cell Components*, 16 February 2011, Available from:
http://www.sglgroup.com/export/sites/sglcarbon/_common/downloads/product/product-groups/su/fuel-cell-components/GDL_34_35_Series_Gas_Diffusion_Layer.pdf

Sinha, P. K., Halleck, P. & Wang, C. Y. (2006). Quantification of liquid water saturation in a PEM fuel cell diffusion medium using X-ray microtomography. *Electrochemical and Solid-State Letters* Vol. 9, No. 7, pp. A344-A348, ISSN 10990062

Taine, J. & Petit, J. P. (1989). *Transferts thermiques, mécanique des fluides anisothermes*, Dunod, ISBN 2-04-018760-X, Paris

Teertstra, P., Karimi, G. & Li, X. (2011). Measurement of in-plane effective thermal conductivity in PEM fuel cell diffusion media. *Electrochimica Acta* Vol. 56, No. 3, pp. 1670-1675, ISSN 00134686

Toray Industries (2005a). Functional and composite properties, In: *Torayca product lineup*, 11 March 2011, Available from:
http://www.torayca.com/techref/en/images/fcp02.html

Toray Industries (2005b). Toray carbon paper, In: *Torayca product lineup*, 16 February 2011, Available from:
http://www.torayca.com/properties/en/images/report_eng09_2.html

Tsushima, S. & Hirai, S. (2011). In situ diagnostics for water transport in proton exchange membrane fuel cells. *Progress in Energy and Combustion Science* Vol. 37, No. 2, pp. 204-220, ISSN 0360-1285

Veyret, D. & Tsotridis, G. (2010). Numerical determination of the effective thermal conductivity of fibrous materials. Application to proton exchange membrane fuel cell gas diffusion layers. *Journal of Power Sources* Vol. 195, No. 5, pp. 1302-1307, ISSN 03787753

Vie, P. J. S. & Kjelstrup, S. (2004). Thermal conductivities from temperature profiles in the polymer electrolyte fuel cell. *Electrochimica Acta* Vol. 49, No. 7, pp. 1069-1077, ISSN 00134686

Wang, J., Carson, J. K., North, M. F. & Cleland, D. J. (2006). A new approach to modelling the effective thermal conductivity of heterogeneous materials. *International Journal of Heat and Mass Transfer* Vol. 49, No. 17-18, pp. 3075-3083, ISSN 00179310

Wang, J., Carson, J. K., North, M. F. & Cleland, D. J. (2008). A new structural model of effective thermal conductivity for heterogeneous materials with co-continuous phases. *International Journal of Heat and Mass Transfer* Vol. 51, No. 9-10, pp. 2389-2397, ISSN 00179310

Wen, C. Y. & Huang, G. W. (2008). Application of a thermally conductive pyrolytic graphite sheet to thermal management of a PEM fuel cell. *Journal of Power Sources* Vol. 178, No. 1, pp. 132-140, ISSN 03787753

Wiegmann, A. & Zemitis, A. (2006). EJ-HEAT: A fast explicit jump harmonic averaging solver for the effective heat conductivity of composite materials. *Fraunhofer ITWM* Vol. 94

Zamel, N., Li, X., Shen, J., Becker, J. & Wiegmann, A. (2010). Estimating effective thermal conductivity in carbon paper diffusion media. *Chemical Engineering Science* Vol. 65, No. 13, pp. 3994-4006, ISSN 00092509

Convection and Conduction Heat Transfer

Edited by Dr. Amimul Ahsan

The convection and conduction heat transfer, thermal conductivity, and phase transformations are significant issues in a design of wide range of industrial processes and devices. This book includes 18 advanced and revised contributions, and it covers mainly (1) heat convection, (2) heat conduction, and (3) heat transfer analysis. The first section introduces mixed convection studies on inclined channels, double diffusive coupling, and on lid driven trapezoidal cavity, forced natural convection through a roof, convection on non-isothermal jet oscillations, unsteady pulsed flow, and hydromagnetic flow with thermal radiation. The second section covers heat conduction in capillary porous bodies and in structures made of functionally graded materials, integral transforms for heat conduction problems, non-linear radiative-conductive heat transfer, thermal conductivity of gas diffusion layers and multi-component natural systems, thermal behavior of the ink, primer and paint, heating in biothermal systems, and RBF finite difference approach in heat conduction. The third section includes heat transfer analysis of reinforced concrete beam, modeling of heat transfer and phase transformations, boundary conditions-surface heat flux and temperature, simulation of phase change materials, and finite element methods of factorial design. The advanced idea and information described here will be fruitful for the readers to find a sustainable solution in an industrialized society.

How to reference

In order to correctly reference this scholarly work, feel free to copy and paste the following:

Andreas Pfrang, Damien Veyret and Georgios Tsotridis (2011). Computation of Thermal Conductivity of Gas Diffusion Layers of PEM Fuel Cells, Convection and Conduction Heat Transfer, Dr. Amimul Ahsan (Ed.), ISBN: 978-953-307-582-2, InTech, Available from: http://www.intechopen.com/books/convection-and-conduction-heat-transfer/computation-of-thermal-conductivity-of-gas-diffusion-layers-of-pem-fuel-cells

INTECH
open science | open minds